RESEARCH ARTICLE | SEPTEMBER 21 2022

Photonic circuits for laser stabilization with integrated ultrahigh Q and Brillouin laser resonators

Kaikai Liu; John H. Dallyn; Grant M. Brodnik; Andrei Isichenko; Mark W. Harrington; Nitesh Chauhan; Debapam Bose; Paul A. Morton; Scott B. Papp; Ryan O. Behunin; Daniel J. Blumenthal ■ ^⑤

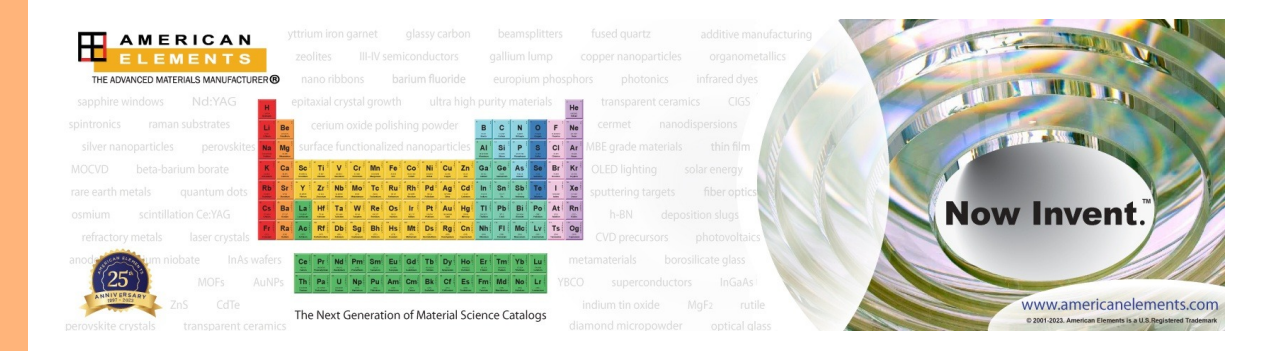


APL Photonics 7, 096104 (2022) https://doi.org/10.1063/5.0091686





CrossMark





Cite as: APL Photon. 7, 096104 (2022); doi: 10.1063/5.0091686 Submitted: 16 March 2022 • Accepted: 24 August 2022 •







Published Online: 21 September 2022

Kaikai Liu,¹ John H. Dallyn,² Grant M. Brodnik,¹ Andrei Isichenko,¹ Mark W. Harrington,¹ Nitesh Chauhan,¹ Debapam Bose,¹ Paul A. Morton,³ Scott B. Papp,^{4,5} Ryan O. Behunin,^{2,6} and Daniel J. Blumenthal^{1,a)}

AFFILIATIONS

- ¹ Department of Electrical and Computer Engineering, University of California Santa Barbara, Santa Barbara, California 93106, USA
- ²Department of Applied Physics and Materials Science, Northern Arizona University, Flagstaff, Arizona 86011, USA
- Morton Photonics, West Friendship, Maryland 21794, USA
- Department of Physics, University of Colorado Boulder, Boulder, Colorado 80309, USA
- ⁵Time and Frequency Division 688, National Institute of Standards and Technology, Boulder, Colorado 80305, USA
- ⁶Center for Materials Interfaces in Research and Applications (¡MIRA!), Northern Arizona University, Flagstaff, Arizona 86011, USA
- a) Author to whom correspondence should be addressed: danb@ucsb.edu

ABSTRACT

The integration of stabilized lasers, sources that generate spectrally pure light, will provide compact, low-cost solutions for applications including quantum information sciences, precision navigation and timing, metrology, and high-capacity fiber communications. We report a significant advancement in this field, demonstrating stabilization of an integrated waveguide Brillouin laser to an integrated waveguide reference cavity, where both resonators are fabricated using the same CMOS-compatible integration platform. We demonstrate reduction of the free running Brillouin laser linewidth to a 292 Hz integral linewidth and carrier stabilization to a 4.9×10^{-13} fractional frequency at 8 ms reaching the cavity-intrinsic thermorefractive noise limit for frequencies down to 80 Hz. We achieve this level of performance using a pair of 56.4×10^6 quality factor Si_3N_4 waveguide ring-resonators that reduce the high-frequency noise by the nonlinear Brillouin process and the low-frequency noise by Pound–Drever–Hall locking to the ultra-low loss resonator. These results represent an important step toward integrated stabilized lasers with reduced sensitivity to environmental disturbances for atomic, molecular, and optical physics (AMO), quantum information processing and sensing, and other precision scientific, sensing, and communications applications.

© 2022 Author(s). All article content, except where otherwise noted, is licensed under a Creative Commons Attribution (CC BY) license (http://creativecommons.org/licenses/by/4.0/). https://doi.org/10.1063/5.0091686

I. INTRODUCTION

Spectrally pure sources are critical for applications that demand low phase noise and high carrier stability, including optical atomic clocks; microwave photonics; optical gyroscopes; quantum systems; atomic, molecular, and optical physics (AMO) and applications; and energy efficient coherent fiber communications applications. Table-scale ultra-stable lasers employ Pound–Drever–Hall (PDH) locking of the laser to a state-of-theart optical reference cavity, delivering linewidths as low as 10 mHz, fractional frequency stability of better than 10^{-15} over ~ 1 s, and high laser output optical power. Such PDH-based designs minimize

cavity thermal noise sources by limiting the intra-cavity optical power and employing a large cavity optical mode volume, athermalized design, and environmental isolation. ^{19,20} In order to bring stabilized laser technology to a wider range of applications, it is critical to implement aspects of these widely employed designs in a CMOS-compatible, wafer-scale, photonic integrated circuit platform that can incorporate other components and functions ^{21–23} for higher-level functionality, to lower cost, size, and weight, and reduce sensitivity to environmental disturbances.

There has been progress toward the miniaturization of stabilized lasers based on PDH feedback designs. Compact, centimeter-

scale whispering gallery mode (WGM) resonators have been used to demonstrate impressive semiconductor laser stabilization, reaching the cavity thermorefractive noise (TRN) stability of 6 \times 10^{-14} at 100 ms.²⁴ A centimeter-scale fused silica cavity was used to stabilize a semiconductor laser to 25 Hz integral linewidth and 1×10^{-13} stability at 20 ms.²⁵ Designs that mitigate high- and low-frequency noise components have been shown to reduce the integral linewidth to 87 Hz and the fundamental linewidth to 3 Hz.²⁶ These bulk-optic reference cavities leverage the well-known inverse relationship between resonator optical mode volume and thermally induced frequency noise^{24,27–29} to lower the TRN floor. However, there has been limited progress in PDH-based laser stabilization using integrated waveguide structures with careful frequency noise and stability measurement and analysis. 30,31 Other well-known approaches to linewidth narrowing include semiconductor laser injection locking^{32–36} based on intra-cavity nonlinear optical feedback to lower the high-frequency noise and mid-range noise down to the resonator-specific TRN floor. 37-40 In general, such injection locking approaches are limited to low laser output power due to unwanted nonlinearities and nonlinear losses as well as power-dependent noise sources [i.e., TRN and photothermal (PT) noise] in the resonator and are not as widely employed in precision scientific systems as PDH systems. PDH stabilization minimizes the optical power into the cavity to mitigate thermally-driven noise and has much more stable frequency noise discrimination compared to injection locking that suffers from frequency noise discrimination instability due to the path length fluctuation between the laser and cavity. 14,39 Therefore, there is a need for photonic integration approaches to PDH cavity stabilized lasers and systems.

In this work, we report a significant advancement in PDHbased photonic integrated laser stabilization, achieved by locking a 1550 nm Si₃N₄ waveguide stimulated Brillouin scattering (SBS) laser to an ultra-low loss \tilde{Si}_3N_4 bus-ring waveguide resonator. We report an integral 292 Hz linewidth and an Allan deviation (ADEV) of 4.9 \times 10⁻¹³ at 8 ms. This is the first demonstration of an integrated SBS laser locking to an integrated reference cavity and represents the best laser stability demonstrated to date for all-waveguide Brillouin and stabilization cavities at the time of the original submission of this manuscript. These results are an important step forward toward demonstrating that an integrated photonic stabilized laser with both narrow fundamental and integral linewidths is within reach. Both integrated resonators, one employed as an active nonlinear SBS laser cavity and the other as a passive reference cavity, are the same large mode volume ($\sim 2 \times 10^6 \ \mu \text{m}^3$) and ultra-high Q waveguide resonator design.⁴¹ The cavities have an intrinsic 56.4×10^6 Q, corresponding to a 0.47 dB/m propagation loss with an absorption-limited loss of 0.05 dB/m. The laser frequency noise is stabilized in two spectral bands, with low frequency noise reduced using PDH locking to the integrated ultra-low loss reference cavity and high frequency noise reduced using the linewidth narrowing properties of the Brillouin laser. 42,43 Our approach is broadly applicable to incorporate other low fundamental linewidth lasers in the first stage^{2,41} including hybrid extended waveguide cavity lasers,^{44,45} and injection locking to high Q resonators⁴⁰ and other low-loss resonator designs^{46,47} in the second stage. We compare the measured stabilized laser frequency noise to calculated PT and TRN and show that the stabilized laser reaches the cavity TRN noise floor down to a 80 Hz frequency offset-from-carrier. This performance is achieved

with the resonators located in an ambient environment with simple passive vibration damping isolation and without vacuum housing or thermal isolation. These results demonstrate the potential to bring PDH stabilized laser designs to photonic integrated wafer-scale compatible solutions, paving the way toward integrated all-waveguide frequency stabilized lasers for AMO, atomic clocks, microwave photonics, precision spectroscopy, and energy-efficient coherent fiber communications. A system-on-chip stabilized laser is possible with other integrated on-chip component technologies. The nonlinear Brillouin and ultra-low loss reference cavities can be combined with integrated PDH locking circuits on silicon⁴⁸ and lead zirconate titanate (PZT) based ring resonator actuators and modulators in the ultra-low loss silicon nitride platform.⁴⁹ Frequency shifting can be realized using an on-chip lithium niobate frequency shifter through electro-optic modulation (EOM).⁵⁰ Potential applications include microring resonator frequency combs, 40,51-53 high-capacity coherent wavelength division multiplexed communications, neutral atom cooling and optical clocks, 1,57,58 and ultra-low phase noise microwave signal generation.²

II. RESULTS

A. Stabilization with nonlinear and ultra-low loss integrated resonators

The process of laser stabilization using nonlinear and ultra-low loss photonic integrated resonators is illustrated in Fig. 1. The output from a pump laser (PL), such as a semiconductor laser [blue arrow in the upper part of Fig. 1(a)], has a typical Gaussian spectral density $S_E(\delta v)$ shown in the blue curve [lower part of Fig. 1(a)]. The pump laser is frequency locked to the nonlinear waveguide resonator to drive the SBS lasing process and reduce the high frequency noise.41 While the fundamental linewidth of first Stokes (S1) emission of the SBS laser is greatly reduced relative to the pump, thermally driven noise processes in the nonlinear cavity lead to low-frequency noise modulation and carrier drift. The nonlinear SBS process reduces the spectral energy in the Lorentzian wings of the S1 line shape, as illustrated in the $S_E(\delta v)$ red curve. A tunable single sideband (SSB), generated from S1 using an acousto-optic modulator (AOM), is frequency locked to the ultra-low loss linear resonator to reduce the close-to-carrier noise energy [Fig. 1(b)]. The low-frequency noise in the SSB is reduced by combining frequency discrimination and PDH locking to the ultra-low loss reference resonator, resulting in a narrowed Gaussian line shape at frequencies near the center carrier frequency [green curve in Fig. 1(b)]. This stabilized laser line shape (green curve) is also illustrated in the frequency noise spectral density plot of Fig. 1(c). The unstabilized pump $[S_E(\delta v), blue]$ high-frequency noise is directly related to its fundamental linewidth and the energy in its line shape wings. The Brillouin lasing action in the nonlinear resonator reduces the highfrequency noise from blue to red (i), reducing the S1 wing spectral energy. The curves in Fig. 1(c) are schematically represented on a log-log plot. At mid- to low-frequencies, the S1 emission spectral energy is dominated by TRN⁶⁰ and PT²⁴ noise sources in the waveguide resonator. Technical noise sources (e.g., vibration and environmental effects) at low frequencies contribute to the Gaussian line shape (red). The TRN in the ultra-low loss stabilization resonator is minimized by maximizing the resonator optical mode volume, and locking is improved by increasing the resonator qualAPL Photonics ARTICLE scitation.org/journal/app

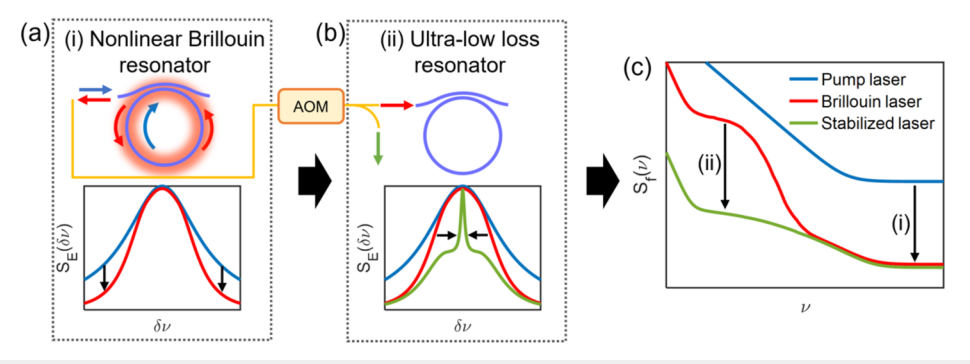


FIG. 1. Illustration of laser stabilization using integrated nonlinear and ultra-low loss resonators. (a) A pump laser (blue arrow) with Gaussian spectral density $S_E(\delta \nu)$ (blue curve) is frequency locked to a nonlinear Brillouin laser resonator. The nonlinear Brillouin process reduces the fundamental linewidth of the input pump laser, producing an output first Stokes (S1) emission (red arrow) that has reduced spectral energy in the Lorentzian wings of the line shape $S_E(\delta \nu)$ (red curve). (b) An acousto-optic modulator (AOM) is used to modulate a tunable single sideband onto S1 that is then frequency locked to the ultra-low loss resonator. The resonator mode volume is large and the optical power kept to a minimum, reducing both the thermorefractive noise (TRN) and photothermal (PT) noise. (c) The frequency noise spectral energy (offset from the carrier) of an unstabilized pump [S_f(ν) blue], reduction of the pump high-frequency noise (i) by the nonlinear resonator Brillouin action (red), and reduction of the lower frequency noise components (ii) by locking the AOM output to the ultra-low loss cavity yielding the noise spectrum [S_f(ν) green]. Both the horizontal and vertical axes in (c) are in a logarithmic scale.

ity factor (Q). The Brillouin output S1 is locked to the ultra-low loss reference resonator using an acousto-optic modulator (AOM) and a high-gain PDH loop to reduce the lower frequency noise components, resulting in a noise spectrum illustrated as green (ii) in Fig. 1(c). The resulting stabilized line shape is characteristic of the green curve in Fig. 1(b).

In this work, the nonlinear Brillouin laser resonator and the ultra-low loss reference cavity are of the same design: a high-aspect ratio silicon nitride (Si₃N₄) waveguide core, 7 µm wide by 40 nm thick, designed to maximize optical mode volume and mitigate losses from sidewall scattering. 61,62 The Brillouin laser resonator radius (11.83 mm) is designed to satisfy the phase matching condition, which for this wavelength occurs at a frequency shift of 10.93 GHz,⁴¹ and is determined by the material properties and waveguide design. An integer multiple of the resonator free spectral range (FSR) is aligned to the S1 frequency shift within the Brillouin gain bandwidth, which in this case is about 150 MHz.⁴¹ The Brillouin lasing threshold is measured to be 10.5 ± 2.2 mW. Throughout this work, the on-chip pump power is maintained at 42 ± 2.2 mW (four times the threshold power) for S1 to operate at just below its clamping point (S2 threshold). The threshold behavior is discussed in more detail in Ref. 41 and details of the resonator design and laser characterization are given in the supplementary material and in Refs. 41, 63, and 64.

The Q factor, optical mode volume, waveguide design, and materials of both resonators are important factors in terms of the Brillouin laser's threshold power and high frequency offset from carrier noise (modified Schawlow–Townes linewidth) and the integral linewidth and fractional frequency noise achieved with the ultra-low loss reference cavity. Both the nonlinear Brillouin resonator and ultra-low loss reference resonators have an intrinsic Q of $56 \pm 1 \times 10^6$ (0.47 dB/m propagation loss) and a loaded Q of $28.2 \pm 0.6 \times 10^6$, which are measured using an electro-optic modulation (EOM) sideband technique (see the supplementary material, Sec. I). Absorption of optical power within the resonators leads to photothermal heating that can produce thermo-optic shifts in the laser frequency. This source of noise plays a critical role at low

frequencies in the reference cavity and hence the stabilized integral linewidth.²⁴ We measure a 0.05 dB/m resonator absorption limited loss that accounts for 10.6% of the total loss, using a photothermal absorption technique (see the supplementary material, Sec. IV). 63,65 The nonlinear Brillouin laser resonator is operated with S1 only emission, just below the second-order Stokes (S2) threshold, with an on-chip pump power of 42 ± 2.2 mW, chosen to minimize the S1 fundamental linewidth. 41,43 This high on-chip pump power in the nonlinear Brillouin cavity combined with the pump laser's relative intensity noise (RIN) induces temperature fluctuations through the absorption heating effect in the nonlinear cavity, which results in PT noise that broadens the free-running Brillouin laser integral linewidth. The PDH lock configuration allows the optical input power to the ultra-low loss reference cavity to be minimized, narrowing the laser integral linewidth to the cavity-intrinsic TRN limit.

B. Brillouin laser stabilization

The stabilized laser experimental setup is shown in Fig. 2(a). The nonlinear Brillouin and ultra-low loss resonators are housed inside passive enclosures to minimize environmental fluctuations, e.g., air flow in the laboratory, and each is mounted on independent temperature-controlled fiber-coupling stages (see the supplementary material, Sec. I, for details). Each chip is mounted on a separate coupling stage in a separate enclosure, with its own coupling fibers and temperature stabilization. The SBS laser output power is 6 ± 1 dBm measured into the fiber (~9 dBm on-chip output optical power and 3 ± 1 dB fiber-to-chip coupling loss) and then passes through an erbium-doped fiber amplifier (EDFA), EOM, AOM, and 90/10 splitter for power amplification and laser frequency stabilization. The SBS laser output in the fiber is amplified with an EDFA to a power level of ~18 dBm. Taking into account the approximate insertion losses of the EOM (5 dB) and AOM (6 dB), the stabilized laser output power after a 90/10 splitter is ~7 dBm (see the supplementary material, Sec. I, for the optical powers and

12 July 2023 15:50:33

APL Photonics ARTICLE scitation.org/journal/app

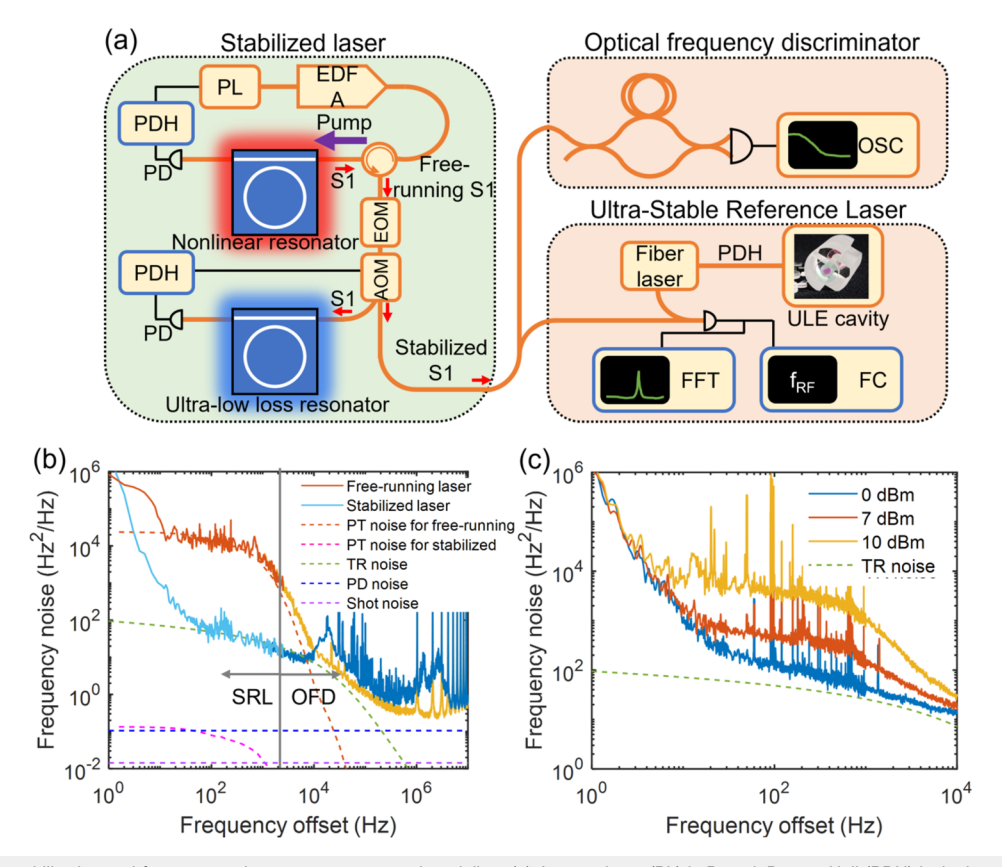


FIG. 2. Brillouin laser stabilization and frequency noise measurements and modeling. (a) A pump laser (PL) is Pound–Drever–Hall (PDH) locked to the nonlinear Brillouin cavity to generate Brillouin first order Stokes (S1) emission. The S1 emission out of the reflection port is PDH locked to the ultra-low loss reference cavity using an acousto-optic modulator (AOM). An optical frequency discriminator (OFD) is used to measure the laser's frequency noise above 1 kHz frequency offset from the carrier, and a heterodyne beatnote from photomixing the Brillouin laser and a stable reference laser (SRL) that is PDH locked to an ultra-stable ultra-low-expansion high-finesse cavity is measured at the frequency counter (FC) for frequency noise measurements below 1 kHz frequency offset from the carrier. SRL, stable reference laser; EDFA, Erbium-doped fiber amplifier; ULE, ultra-low expansion; OSC, oscilloscope; PD, photodetector. (b) OFD and SRL frequency noise measurements for the free-running and stabilized Brillouin laser with the modeled photothermal (PT) noise and thermorefractive (TR) noise in the nonlinear and reference cavities and photodetector (PD) and shot noise in the PDH lock loop. (c) Frequency noise below 10 kHz offset for the stabilized laser measured by the SRL method increases with the on-chip input power in the reference resonator, as more on-chip input increases the temperature fluctuation variance defined as PT noise. The on-chip power for the blue, orange, and yellow curves is experimentally calibrated to be 0, 7, and 10 ± 1 dBm.

insertion losses in the PDH lock). The free-running Brillouin S1 emission is generated by PDH locking the pump laser to the SBS resonator. The on-chip pump power is maintained at 42 ± 2.2 mW such that S1 operates just below its clamping point. The Brillouin S1 emission is then modulated using an AOM driven by a voltage-controlled oscillator (VCO) and PDH locked to the reference cavity, with an on-chip power of –10 dBm and a lock loop bandwidth of ~20 kHz. An unbalanced fiber Mach–Zehnder interferometer (MZI) with a 1.026 MHz FSR is used as an optical frequency discriminator (OFD) to measure the frequency noise above ~1 kHz offset from the carrier. Hz frequency noise below ~1 kHz frequency offset from carrier, we heterodyne the stabilized S1 with a reference RockTM single frequency fiber laser that is PDH locked to a Stable Laser SystemsTM ultra-low-expansion (ULE) high-finesse cavity. The reference laser has a Hz-level linewidth output at 1550 nm wavelength, with a frequency drift of ~0.1 Hz/s and frequency stability

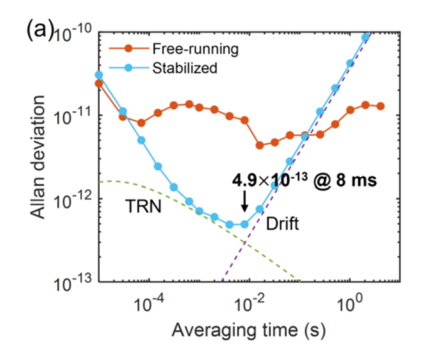
of $\sim 10^{-15}$ at 1 s averaging time. We refer to this reference laser as the stable reference laser (SRL) and the frequency noise measurement using this laser as the SRL frequency noise measurement. The stabilized Brillouin S1 is photomixed with the SRL output to produce a heterodyne signal that carries the Brillouin laser's frequency noise combined with the noise of the VCO-driven AOM. The resulting heterodyne signal, an ~100 MHz beatnote, is characterized using a Keysight 53230A frequency counter (FC) with a frequency noise floor below 10^{-3} Hz²/Hz. The combination of the SRL frequency stability below a 1 kHz offset and the frequency noise floor of the frequency counter below 10⁻³ Hz²/Hz enables accurate measurement of both the free-running and stabilized Brillouin laser emission at frequencies below 1 kHz. The OFD and SRL frequency noise measurements and the impact of VCO and AOM are discussed in detail in the supplementary material, Sec. III. The laser frequency noise measurements are shown in Fig. 2(b) yielding the free-running and

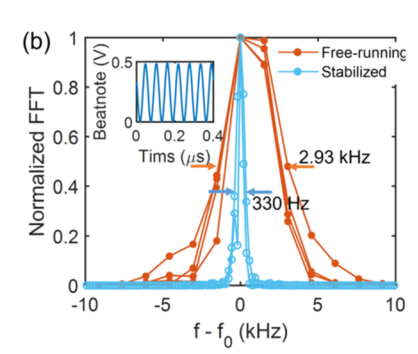
stabilized Brillouin laser fundamental linewidths of 0.72 and 1.6 Hz, respectively. The frequency noise spectra are plotted in Fig. 2(b) with 60 and 120 Hz tones removed. Figure S3(c) in the supplementary shows the original frequency noise spectra with the 60 and 120 Hz tones. The increase in high-frequency noise is due to added phase noise from the VCO that in turn drives the AOM (see the supplementary material, Sec. I, for more discussion on the VCO-added phase noise).

The integral linewidths are calculated from the frequency noise spectrum for the free-running and stabilized Brillouin laser. A factor of 10 decrease is measured in the stabilized linewidth over the free-running linewidth, at 292 Hz and 3.24 kHz, respectively (see the supplementary material, Sec. II, for the integral linewidth calculation). The increase in the high-frequency noise in the AOMmodulated S1 output is due to the Brillouin laser fundamental linewidth being lower than that of the AOM and its VCO. The stabilized S1 frequency noise is close to the resonator-intrinsic TRN limit for frequencies from 80 Hz to 10 kHz, as shown in Fig. 2(b). The overlapping ADEV shown in Fig. 3(a) is calculated from the time trace of heterodyne frequency recorded by the frequency counter, which for the stabilized Brillouin laser reaches a minimum of 4.9 $\times~10^{-13}$ at 8 ms averaging time. While the $1/\pi$ integral linewidth of 292 Hz for the stabilized laser does not take an averaging time into account, the measured ADEV at 8 ms does, and therefore, correlates the linewidth contributions at 8 ms to the integral linewidth before the linewidth becomes drift dominated. The TRN sets a lower limit for the stabilized ADEV at averaging times up to around 5 ms, while, outside this range, other noise sources dominate the ADEV. The random walk frequency noise (drift), estimated to be 10 kHz/s over the time scale of several seconds, dominates the linewidth at ADEV averaging times longer than 10 ms [right-hand upward purple-dashed curve in Fig. 3(a)]. As shown in Fig. 3(b), the Fourier transform of the SRL and the Brillouin laser heterodyne beatnote yields linewidths of 330 Hz for the stabilized and 2.93 kHz for the free-running Brillouin laser. These values are in good agreement with our calculated integral linewidths from the frequency noise spectrum.¹⁸ The heterodyne beatnote frequency recorded by the counter over a 1-second period [Fig. 3(c)] shows the improvement in laser frequency fluctuation when the Brillouin laser is cavity stabilized over the free-running laser.

C. Frequency noise

The noise sources and PDH parameters determine the role that the nonlinear Brillouin and ultra-low loss reference cavities play in laser stabilization. The noise sources include shot noise, photodetector noise, PT noise, and TRN [see Fig. 2(b)]. The PT noise and TRN are the dominant contributions to the thermally driven frequency instability within both the nonlinear Brillouin and ultra-low loss reference resonators: (i) TRN arises from fundamental thermodynamic fluctuations of solids and (ii) PT noise is produced by thermal fluctuations driven by power absorbed from a fluctuating optical field. 60,67 In the nonlinear resonator, the dominant noise contribution is PT noise induced by fluctuations in the high on-chip pump power. However, in the ultra-low loss reference resonator, TRN is the dominant noise contribution, enabling the high gain and moderate bandwidth PDH loop to stabilize the laser to the TRN limit down to about 80 Hz. The shot and detector noise in Fig. 2(b) are below the TRN limit and are calculated using Refs. 60 and 67. The TRN is the same for both the nonlinear and reference resonators, as both resonators have the same physical parameters, while the PT noise is dependent on the on-chip optical power and optical power fluctuations. To model the PT noise, we include spatial changes in the temperature field produced by fluctuations in absorbed power.⁶⁷ The inputs to our frequency noise model include the pump laser and Brillouin laser RIN (shown in the supplementary material, Sec. IV), the on-chip free running Brillouin laser input pump power, the reference cavity on-chip input power, the resonator optical absorption loss as measured by the photothermal technique, the cavity buildup factor, and optical mode profiles.⁶⁷ Our modeling shows that the free-running Brillouin laser frequency noise at low-frequency offset (10 Hz-10 kHz) is dominated by PT noise [orange-dashed curve in Fig. 2(b)]. The simulation also predicts that ultra-low loss reference cavity frequency noise is limited by the TRN [green-dashed curve





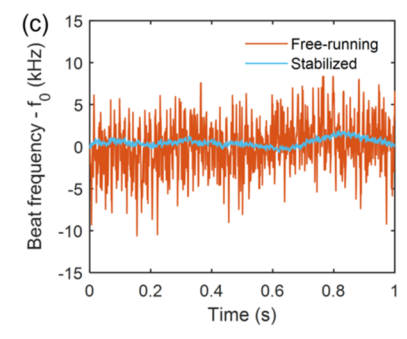


FIG. 3. Stabilized laser Allan deviation (ADEV) and linewidth. (a) The stabilized Brillouin laser reaches a minimum ADEV of 4.9×10^{-13} at 8 ms (blue lower curve) while the free-running Brillouin laser. The overlapping ADEV is calculated from the heterodyne beatnote frequency from photomixing the Brillouin laser and the stable reference laser (SLR) and recorded by the frequency counter. (b) The Fast Fourier transform (FFT) of the heterodyne signal reveals the linewidths, with a resolution bandwidth (RBW) of 1 kHz for the orange curve and 100 Hz for the blue curve. (c) A 1-s time trace of the heterodyne beatnote frequency shows the fluctuation of the laser frequency with and without reference cavity stabilization. The heterodyne frequency is recorded by the frequency counter with a sampling rate of 1 kHz and the center frequencies (f_0) for the orange and blue curves are ~162 and ~156 MHz, respectively.

TABLE I. Comparison of stabilization using miniaturized and integrated cavities. Fundamental linewidth Δv_F and integral linewidth Δv_F

Cavity type	Bulk/integrated	Environmental isolation	Δu_F	Δv_I	Allan deviation (ADEV)	Reference
WGM	Bulk	Vacuum housing		20 Hz	6×10^{-14} at 100 ms	24
Microrod Fabry-Pérot	Bulk	Vibration-immune holding structure		25 Hz	1×10^{-13} at 20 ms	25
Microdisk, microrod	Bulk	Temperature control and enclosure	3 Hz	87 Hz		26
Etched silica spiral on silicon		Acoustic shielding		Several 100 Hz	3.9×10^{-13} at 0.4 ms 1.6×10^{-12} at 8 ms	30
Waveguide microring	Integrated	Temperature control and enclosure	160 kHz	~1 kHz		31
Waveguide ring resonator	Integrated	Temperature control and enclosure	1.6 Hz	292 Hz	4.9×10^{-13} at 8 ms	This work

in Fig. 2(b)] at a frequency offset above 10 Hz. This results in the TRN setting the fundamental noise limit for the stabilized laser at offset frequencies between 100 Hz and 10 kHz. To assess the effect of on-chip power on the PT noise in the reference cavity, we vary the fiber-coupled input power between three values: 0, 7, and 10 dBm, and measure the frequency noise as shown in Fig. 2(c). Since the PT noise is proportional to the square of the on-chip input power,⁶⁷ limiting the chip input power to 0.1 mW will maintain TRN-limited operation, which is consistent with the conclusion drawn from our PT noise modeling.

III. DISCUSSION AND CONCLUSION

We report a photonic integrated stabilized Brillouin laser, where both the Brillouin laser and the stabilization cavity are implemented in photonic integrated waveguide devices for the first time. The laser measures a narrow 292 Hz integral linewidth with a frequency stability of 4.9 $\times~10^{-13}$ at 8 ms, the lowest linewidth and laser stability demonstrated for all-waveguide Brillouin and stabilization cavities, at the time of the original submission of this manuscript.

The nonlinear and reference cavity configuration reduces the noise in frequency bands using identical 56.4×10^6 intrinsic Q photonic integrated bus-coupled microring resonators. Measurements and simulations of the cavity frequency noise dynamics, including the cavity-intrinsic TRN, the on-chip power fluctuation induced PT noise, as well as the technical noise of the PDH locking loop, show that laser emission stabilization is limited by the cavity intrinsic TRN for frequencies as low as 80 Hz, while the ambient environmental noise, such as the thermal drift, becomes dominant at frequencies below 80 Hz, and the high frequency offset from carrier noise is determined by the Brillouin laser. A summary of these

results compared to the bulk optic and miniaturized PDH stabilization approaches is given in Table I, showing that our integrated stabilized laser performance is reaching similar performance. The averaging time at which the minimum ADEV occurs and the frequency noise and ADEV measurements relative to the cavity TRN limit are important. For example, the jitter-dominated linewidth reported here occurs at over an order of magnitude longer averaging time than the jitter-dominated 0.4 ms reported in Ref. 30. Comparing the linewidths at 8 ms, the stabilized fiber laser fractional frequency noise reported in Ref. 30 increases to 1.6×10^{-12} , corresponding to a drift-dominated 310 Hz linewidth. Additionally, we report the TRN limited performance down to 80 Hz, a measurement that has not previously been reported for integrated stabilization cavities.

In addition to the optical frequency noise and stability characteristics, the optical output power is an important parameter for many applications, including optical sensing and gyroscopes, 4,5 optical coherent communications, ¹³ and optical nonlinear processes, such as microcomb generation. ⁵² In the future, the output power of this stabilized Brillouin laser can be increased through the integration of all components, including modulators, frequency shifters, and splitters and combiners. Additionally, the output power of the Brillouin laser can be increased using techniques such as higherorder Stokes inhibition. 68-70 Recently, we have demonstrated an integrated cascade-inhibited Brillouin laser with a 2.3 mW threshold that outputs 10 mW of optical power, 70 which can eliminate the need for optical amplifiers for this laser in future fully integrated systems. With various other integrated on-chip component technologies such as integrated PDH locking circuits on silicon,48 PZT actuators and modulators in the ultra-low loss Si₃N₄ platform, ⁴⁹ on-chip lithium niobate frequency shifter,⁵⁰ a system-on-chip stabilized laser with narrow integral and fundamental linewidths and high output power is possible.

The PT and technical noise in the lock loop and on-chip input power to the reference cavity are critical factors in linewidth reduction and the Q factor is critical for both the Brillouin lasing emission and laser stabilization. The Brillouin lasing threshold is inversely proportional to Q², so a higher Q lowers the Brillouin laser threshold and intracavity power fluctuations, leading to reduced PT noise. Under cavity locking, Q determines the signal-to-noise ratio in the frequency discrimination of the laser frequency against the cavity resonance, which is proportional to Q and the optical input power. A high Q factor is required to tightly lock the nonlinear cavity output to the reference cavity with small optical input power, such that the PDH lock is not limited by technical noise or the PT noise induced by the optical input power fluctuations. Under these conditions, laser stabilization performance is limited by the reference cavity itself and the environmental noise. While identical in geometry and optical properties, there are differences in the thermally driven noise processes in the nonlinear and reference cavities due to intra-cavity power levels. This frequency noise difference can be decreased in the future by reducing the Brillouin laser threshold with increased cavity Q.64 Future improvements could include increasing the optical mode volume by using a longer resonator. These results show promise to integrate stabilized lasers using waferscale, CMOS compatible, photonic integration, paving the way to scale for compact precision sources for atomic and molecular scientific experiments as well as enabling portable solutions for precision applications.

SUPPLEMENTARY MATERIAL

More details of the resonator design and fabrication, PDH lock setup, frequency noise modeling, and analysis can be found in the supplementary material.

ACKNOWLEDGMENTS

This work was supported by the Advanced Research Projects Agency-Energy (ARPA-E), U.S. Department of Energy, under the OPEN-2018 Program Award No. DE-AR0001042 and the DARPA GRYPHON Program Contract No. HR0011-22-2-0008. The views and conclusions contained in this document are those of the authors and should not be interpreted as representing official policies of ARPA-E or the U.S. Government or any agency thereof. Andrei Isichenko acknowledges the support from the National Defense Science and Engineering Graduate (NDSEG) Fellowship Program.

AUTHOR DECLARATIONS

Conflict of Interest

The authors have no conflicts to disclose.

Author Contributions

Kaikai Liu: Conceptualization (equal); Investigation (lead); Writing – original draft (equal); Writing – review & editing (equal). **Ryan O. Behunin**: Conceptualization (equal); Formal analysis

(equal); Funding acquisition (equal); Investigation (equal); Methodology (equal); Resources (equal); Supervision (equal). Daniel J. Blumenthal: Conceptualization (equal); Formal analysis (equal); Funding acquisition (equal); Investigation (equal); Methodology (equal); Project administration (equal); Resources (equal); Supervision (equal); Writing - original draft (equal); Writing - review & editing (equal). John H. Dallyn: Formal analysis (supporting); Methodology (supporting); Software (equal). Grant M. Brodnik: Conceptualization (equal); Investigation (supporting); Methodology (equal). Andrei Isichenko: Data curation (equal); Formal analysis (equal); Investigation (equal); Software (equal). Mark W. Harrington: Conceptualization (supporting); Investigation (supporting); Software (supporting). Nitesh Chauhan: Formal analysis (supporting); Investigation (supporting); Methodology (equal); Resources (supporting); Software (supporting). Debapam Bose: Investigation (equal); Resources (supporting). Paul A. Morton: Conceptualization (supporting); Formal analysis (supporting); Investigation (supporting); Resources (supporting); Writing - original draft (equal). Scott B. Papp: Conceptualization (equal); Formal analysis (equal); Funding acquisition (equal); Investigation (equal); Project administration (equal); Resources (equal); Supervision (equal).

DATA AVAILABILITY

The data that support the findings of this study are available from the corresponding author upon reasonable request.

REFERENCES

- ¹ A. D. Ludlow, M. M. Boyd, J. Ye, E. Peik, and P. O. Schmidt, "Optical atomic clocks," Rev. Mod. Phys. **87**, 637–701 (2015).
- ²P. A. Morton and M. J. Morton, "High-power, ultra-low noise hybrid lasers for microwave photonics and optical sensing," J. Lightwave Technol. **36**, 5048–5057 (2018).
- ³ J. Li, H. Lee, and K. J. Vahala, "Microwave synthesizer using an on-chip Brillouin oscillator," Nat. Commun. **4**, 2097 (2013).
- ⁴B. Culshaw, "The optical fibre Sagnac interferometer: An overview of its principles and applications," Meas. Sci. Technol. 17, R1–R16 (2006).
- ⁵S. Gundavarapu, M. Belt, T. A. Huffman, M. A. Tran, T. Komljenovic, J. E. Bowers, and D. J. Blumenthal, "Interferometric optical gyroscope based on an integrated Si₃N₄ low-loss waveguide coil," J. Lightwave Technol. **36**, 1185–1191 (2018).
- ⁶Y.-H. Lai, M.-G. Suh, Y.-K. Lu, B. Shen, Q.-F. Yang, H. Wang, J. Li, S. H. Lee, K. Y. Yang, and K. Vahala, "Earth rotation measured by a chip-scale ring laser gyroscope," Nat. Photonics 14, 345–349 (2020).
- ⁷A. Orieux and E. Diamanti, "Recent advances on integrated quantum communications," J. Opt. 18, 083002 (2016).
- ⁸M. Mamaev, R. Blatt, J. Ye, and A. M. Rey, "Cluster state generation with spinorbit coupled fermionic atoms in optical lattices," Phys. Rev. Lett. **122**, 160402 (2019).
- ⁹J. L. Bohn, A. M. Rey, and J. Ye, "Cold molecules: Progress in quantum engineering of chemistry and quantum matter," Science 357, 1002–1010 (2017).
- ¹⁰D. S. Jin and J. Ye, "Introduction to ultracold molecules: New frontiers in quantum and chemical physics," Chem. Rev. **112**, 4801–4802 (2012).
- 11 S. Ding, Y. Wu, I. A. Finneran, J. J. Burau, and J. Ye, "Sub-Doppler cooling and compressed trapping of YO molecules at μ K temperatures," Phys. Rev. X 10, 021049 (2020)
- ¹²D. J. Blumenthal, H. Ballani, R. O. Behunin, J. E. Bowers, P. Costa, D. Lenoski, P. A. Morton, S. B. Papp, and P. T. Rakich, "Frequency stabilized links for coherent

- WDM fiber interconnects in the datacenter," J. Lightwave Technol. 38, 3376–3386 (2020).
- ¹³ K. Kikuchi, "Fundamentals of coherent optical fiber communications," J. Lightwave Technol. 34, 157–179 (2016).
- ¹⁴E. D. Black, "An introduction to Pound-Drever-Hall laser frequency stabilization," Am. J. Phys. 69, 79-87 (2000).
- ¹⁵Y. Y. Jiang, A. D. Ludlow, N. D. Lemke, R. W. Fox, J. A. Sherman, L.-S. Ma, and C. W. Oates, "Making optical atomic clocks more stable with 10⁻¹⁶-level laser stabilization," Nat. Photonics 5, 158–161 (2011).
- ¹⁶T. Kessler, C. Hagemann, C. Grebing, T. Legero, U. Sterr, F. Riehle, M. J. Martin, L. Chen, and J. Ye, "A sub-40-mHz-linewidth laser based on a silicon single-crystal optical cavity," Nat. Photonics 6, 687–692 (2012).
- ¹⁷S. Hirata, T. Akatsuka, Y. Ohtake, and A. Morinaga, "Sub-hertz-linewidth diode laser stabilized to an ultralow-drift high-finesse optical cavity," Appl. Phys. Express 7, 022705 (2014).
- ¹⁸D. G. Matei, T. Legero, S. Häfner, C. Grebing, R. Weyrich, W. Zhang, L. Sonderhouse, J. M. Robinson, J. Ye, F. Riehle, and U. Sterr, "1.5 μm lasers with sub-10 mHz linewidth," Phys. Rev. Lett. 118, 263202 (2017).
- ¹⁹K. Numata, A. Kemery, and J. Camp, "Thermal-noise limit in the frequency stabilization of lasers with rigid cavities," Phys. Rev. Lett. 93, 250602 (2004).
- ²⁰ M. Notcutt, L.-S. Ma, A. D. Ludlow, S. M. Foreman, J. Ye, and J. L. Hall, "Contribution of thermal noise to frequency stability of rigid optical cavity via Hertz-linewidth lasers," Phys. Rev. A 73, 031804 (2006).
- ²¹ M. H. P. Pfeiffer, A. Kordts, V. Brasch, M. Zervas, M. Geiselmann, J. D. Jost, and T. J. Kippenberg, "Photonic Damascene process for integrated high-Q microresonator based nonlinear photonics," Optica 3, 20–25 (2016).
- ²²D. J. Blumenthal, R. Heideman, D. Geuzebroek, A. Leinse, and C. Roeloffzen, "Silicon nitride in silicon photonics," Proc. IEEE 106, 2209–2231 (2018).
- ²³ D. Marpaung, J. Yao, and J. Capmany, "Integrated microwave photonics," Nat. Photonics 13, 80–90 (2019).
- ²⁴J. Alnis, A. Schliesser, C. Y. Wang, J. Hofer, T. J. Kippenberg, and T. W. Hänsch, "Thermal-noise-limited crystalline whispering-gallery-mode resonator for laser stabilization," Phys. Rev. A 84, 011804 (2011).
- ²⁵ W. Zhang, L. Stern, D. Carlson, D. Bopp, Z. Newman, S. Kang, J. Kitching, and S. B. Papp, "Ultranarrow linewidth photonic-atomic laser," Laser Photonics Rev. 14, 1900293 (2020).
- ²⁶W. Loh, A. A. S. Green, F. N. Baynes, D. C. Cole, F. J. Quinlan, H. Lee, K. J. Vahala, S. B. Papp, and S. A. Diddams, "Dual-microcavity narrow-linewidth Brillouin laser," Optica **2**, 225–232 (2015).
- ²⁷G. Huang, E. Lucas, J. Liu, A. S. Raja, G. Lihachev, M. L. Gorodetsky, N. J. Engelsen, and T. J. Kippenberg, "Thermorefractive noise in silicon-nitride microresonators," Phys. Rev. A 99, 061801 (2019).
- ²⁸ A. B. Matsko, A. A. Savchenkov, N. Yu, and L. Maleki, "Whispering-gallery-mode resonators as frequency references. I. Fundamental limitations," J. Opt. Soc. Am. B **24**, 1324 (2007).
- ²⁹ A. A. Savchenkov, A. B. Matsko, V. S. Ilchenko, N. Yu, and L. Maleki, "Whispering-gallery-mode resonators as frequency references. II. Stabilization," J. Opt. Soc. Am. B 24, 2988 (2007).
- ³⁰ H. Lee, M.-G. Suh, T. Chen, J. Li, S. A. Diddams, and K. J. Vahala, "Spiral resonators for on-chip laser frequency stabilization," Nat. Commun. 4, 2468 (2013).
- 31 D. T. Spencer, M. L. Davenport, T. Komljenovic, S. Srinivasan, and J. E. Bowers, "Stabilization of heterogeneous silicon lasers using Pound-Drever-Hall locking to Si_3N_4 ring resonators," Opt. Express $\bf 24$, 13511–13517 (2016).
- ³²T. Ohta, S. Makino, H. Nakano, S. Endo, and S. Ono, "New self-injection oscillator using directional filter," in *1973 3rd European Microwave Conference* (IEEE, 1973), Vol. 1, pp. 1–4.
- ³³ H. Li and N. B. Abraham, "Power spectrum of frequency noise of semiconductor lasers with optical feedback from a high-finesse resonator," Appl. Phys. Lett. **53**, 2257–2259 (1988).
- ³⁴D. R. Hjelme, A. R. Mickelson, and R. G. Beausoleil, "Semiconductor laser stabilization by external optical feedback," IEEE J. Quantum Electron. **27**, 352–372 (1991).

- ³⁵R. R. Galiev, N. M. Kondratiev, V. E. Lobanov, A. B. Matsko, and I. A. Bilenko, "Optimization of laser stabilization via self-injection locking to a whispering-gallery-mode microresonator," Phys. Rev. Appl 14, 014036 (2020).
- ³⁶P. Laurent, A. Clairon, and C. Breant, "Frequency noise analysis of optically self-locked diode lasers," IEEE J. Quantum Electron. **25**, 1131–1142 (1989).
- ³⁷L. Hao, X. Wang, D. Guo, K. Jia, P. Fan, J. Guo, X. Ni, G. Zhao, Z. Xie, and S.-n. Zhu, "Narrow-linewidth self-injection locked diode laser with a high-Q fiber Fabry–Perot resonator," Opt. Lett. **46**, 1397 (2021).
- ³⁸ A. A. Savchenkov, S.-W. Chiow, M. Ghasemkhani, S. Williams, N. Yu, R. C. Stirbl, and A. B. Matsko, "Self-injection locking efficiency of a UV Fabry–Perot laser diode," Opt. Lett. **44**, 4175–4178 (2019).
- ³⁹ N. M. Kondratiev, V. E. Lobanov, A. V. Cherenkov, A. S. Voloshin, N. G. Pavlov, S. Koptyaev, and M. L. Gorodetsky, "Self-injection locking of a laser diode to a high-Q WGM microresonator," Opt. Express 25, 28167–28178 (2017).
- ⁴⁰W. Jin, Q.-F. Yang, L. Chang, B. Shen, H. Wang, M. A. Leal, L. Wu, M. Gao, A. Feshali, M. Paniccia, K. J. Vahala, and J. E. Bowers, "Hertz-linewidth semiconductor lasers using CMOS-ready ultra-high-Q microresonators," Nat. Photonics 15, 346–353 (2021).
- ⁴¹S. Gundavarapu, G. M. Brodnik, M. Puckett, T. Huffman, D. Bose, R. Behunin, J. Wu, T. Qiu, C. Pinho, N. Chauhan, J. Nohava, P. T. Rakich, K. D. Nelson, M. Salit, and D. J. Blumenthal, "Sub-hertz fundamental linewidth photonic integrated Brillouin laser," Nat. Photonics 13 (2018).
- ⁴²A. Debut, S. Randoux, and J. Zemmouri, "Linewidth narrowing in Brillouin lasers: Theoretical analysis," Phys. Rev. A 62, 023803 (2000).
- ⁴³R. O. Behunin, N. T. Otterstrom, P. T. Rakich, S. Gundavarapu, and D. J. Blumenthal, "Fundamental noise dynamics in cascaded-order Brillouin lasers," Phys. Rev. A 98, 023832 (2018).
- ⁴⁴C. Xiang, J. Guo, W. Jin, L. Wu, J. Peters, W. Xie, L. Chang, B. Shen, H. Wang, Q.-F. Yang, D. Kinghorn, M. Paniccia, K. J. Vahala, P. A. Morton, and J. E. Bowers, "High-performance lasers for fully integrated silicon nitride photonics," Nat. Commun. 12, 6650 (2021).
- 45 Y. Fan, A. van Rees, P. J. M. van der Slot, J. Mak, R. M. Oldenbeuving, M. Hoekman, D. Geskus, C. G. H. Roeloffzen, and K.-J. Boller, "Hybrid integrated InP-Si₃N₄ diode laser with a 40-Hz intrinsic linewidth," Opt. Express **28**, 021713 (2020).
- ⁴⁶J. Wu, T. Moein, X. Xu, G. Ren, A. Mitchell, and D. J. Moss, "Micro-ring resonator quality factor enhancement via an integrated Fabry-Perot cavity," APL Photonics 2, 056103 (2017).
- ⁴⁷S. Zheng, Z. Ruan, S. Gao, Y. Long, S. Li, M. He, N. Zhou, J. Du, L. Shen, X. Cai, and J. Wang, "Compact tunable electromagnetically induced transparency and Fano resonance on silicon platform," Opt. Express 25, 25655–25662 (2017).
- ⁴⁸ M. H. Idjadi and F. Aflatouni, "Integrated Pound-Drever-Hall laser stabilization system in silicon," Nat. Commun. 8, 1209 (2017).
- ⁴⁹ J. Wang, K. Liu, M. W. Harrington, R. Q. Rudy, and D. J. Blumenthal, "Ultra-low loss silicon nitride ring modulator with low power PZT actuation for photonic control," in *Optical Fiber Communication Conference (OFC) 2022* (Optica Publishing Group, 2022), p. W3D.5.
- ⁵⁰Y. Hu, M. Yu, D. Zhu, N. Sinclair, A. Shams-Ansari, L. Shao, J. Holzgrafe, E. Puma, M. Zhang, and M. Lončar, "On-chip electro-optic frequency shifters and beam splitters," Nature 599, 587–593 (2021).
- ⁵¹T. J. Kippenberg, A. L. Gaeta, M. Lipson, and M. L. Gorodetsky, "Dissipative Kerr solitons in optical microresonators," Science 361, eaan8083 (2018).
- ⁵²L. Chang, S. Liu, and J. E. Bowers, "Integrated optical frequency comb technologies," Nat. Photonics 16, 95–108 (2022).
- ⁵³ J. Liu, E. Lucas, A. S. Raja, J. He, J. Riemensberger, R. N. Wang, M. Karpov, H. Guo, R. Bouchand, and T. J. Kippenberg, "Photonic microwave generation in the X- and K-band using integrated soliton microcombs," Nat. Photonics 14, 486–491 (2020).
- ⁵⁴G. M. Brodnik, M. W. Harrington, D. Bose, A. M. Netherton, W. Zhang, L. Stern, P. A. Morton, J. E. Bowers, S. B. Papp, and D. J. Blumenthal, "Chipscale, optical-frequency-stabilized PLL for DSP-free, low-power coherent QAM in the DCI," in *Optical Fiber Communication Conference (OFC) 2020* (OSA, 2020), p. M3A.6.

APL Photonics ARTICLE scitation.org/journal/app

- ⁵⁵P. Marin-Palomo, J. N. Kemal, M. Karpov, A. Kordts, J. Pfeifle, M. H. P. Pfeiffer, P. Trocha, S. Wolf, V. Brasch, M. H. Anderson, R. Rosenberger, K. Vijayan, W. Freude, T. J. Kippenberg, and C. Koos, "Microresonator-based solitons for massively parallel coherent optical communications," Nature 546, 274–279 (2017).
- ⁵⁶B. Corcoran, M. Tan, X. Xu, A. Boes, J. Wu, T. G. Nguyen, S. T. Chu, B. E. Little, R. Morandotti, A. Mitchell, and D. J. Moss, "Ultra-dense optical data transmission over standard fibre with a single chip source," Nat. Commun. 11, 2568 (2020).
- ⁵⁷N. Chauhan, D. Bose, M. Puckett, R. Moreira, K. Nelson, and D.. J. Blumenthal, "Photonic integrated Si₃N₄ ultra-large-area grating waveguide MOT interface for 3D atomic clock laser cooling," in *Conference on Lasers and Electro-Optics* (OSA, 2019), p. STu4O.3, https://doi.org/10.1364/cleo_si.2019.stu4O.3.
- ⁵⁸ W. Loh, S. Yegnanarayanan, F. O'Donnell, and P. W. Juodawlkis, "Ultra-narrow linewidth Brillouin laser with nanokelvin temperature self-referencing," Optica **6**, 152 (2019).
- ⁵⁹Z. Yuan, H. Wang, L. Wu, M. Gao, and K. Vahala, "Linewidth enhancement factor in a microcavity Brillouin laser," Optica 7, 1150–1153 (2020).
- ⁶⁰M. L. Gorodetsky and I. S. Grudinin, "Fundamental thermal fluctuations in microspheres," J. Opt. Soc. Am. B 21, 697 (2004).
- ⁶¹ J. F. Bauters, M. J. R. Heck, D. John, D. Dai, M.-C. Tien, J. S. Barton, A. Leinse, R. G. Heideman, D. J. Blumenthal, J. E. Bowers, F. Burmeister, J. P. Mack, H. N. Poulsen, M. L. Masanović, B. Stamenić, D. J. Blumenthal, J. E. Bowers, B. Larsen, L. Nielsen, K. Zenth, L. Leick, C. Laurent-Lund, L. Andersen, and K. Mattsson, "Ultra-low-loss high-aspect-ratio Si₃N₄ waveguides," Opt. Express 19, 3163 (2011).
- 62 D. T. Spencer, J. F. Bauters, M. J. R. Heck, and J. E. Bowers, "Integrated waveguide coupled $\rm Si_3N_4$ resonators in the ultrahigh-Q regime," Optica 1, 153 (2014).

- ⁶³ M. W. Puckett, K. Liu, N. Chauhan, Q. Zhao, N. Jin, H. Cheng, J. Wu, R. O. Behunin, P. T. Rakich, K. D. Nelson, and D. J. Blumenthal, "422 Million intrinsic quality factor planar integrated all-waveguide resonator with sub-MHz linewidth," Nat. Commun. 12, 934 (2021).
- 64 K. Liu, N. Jin, H. Cheng, N. Chauhan, M. W. Puckett, K. D. Nelson, R. O. Behunin, P. T. Rakich, and D. J. Blumenthal, "Ultralow 0.034 dB/m loss wafer-scale integrated photonics realizing 720 million Q and 380 μW threshold Brillouin lasing," Opt. Lett. 47, 1855 (2022).
- ⁶⁵M. H. P. Pfeiffer, J. Liu, A. S. Raja, T. Morais, B. Ghadiani, and T. J. Kippenberg, "Ultra-smooth silicon nitride waveguides based on the damascene reflow process: Fabrication and loss origins," Optica 5, 884 (2018).
- ⁶⁶J. Li, H. Lee, T. Chen, and K. J. Vahala, "Characterization of a high coherence, Brillouin microcavity laser on silicon," Opt. Express **20**, 020170 (2012).
- ⁶⁷J. H. Dallyn, K. Liu, M. W. Harrington, G. M. Brodnik, P. T. Rakich, D. J. Blumenthal, and R. O. Behunin, "Thermal and driven noise in Brillouin lasers," Phys. Rev. A 105, 043506 (2022).
- ⁶⁸H. Wang, L. Wu, Z. Yuan, and K. Vahala, "Towards milli-Hertz laser frequency noise on a chip," in 2021 Conference on Lasers and Electro-Optics (CLEO) (OPTICA, 2021), pp. 1–2.
- ⁶⁹Y. Qin, S. Ding, M. Zhang, Y. Wang, Q. Shi, Z. Li, J. Wen, M. Xiao, and X. Jiang, "High-power, low-noise Brillouin laser on a silicon chip," Opt. Lett. **47**, 1638 (2022).
- ⁷⁰ K. Liu, M. W. Harrington, K. D. Nelson, R. O. Behunin, S. B. Papp, and D. J. Blumenthal, "Photonic integrated cascade-inhibited Brillouin laser with sub-100-mHz fundamental linewidth," in *Conference on Lasers and Electro-Optics* (OSA, 2022), p. SF2K.1.